Available online at www.eccomasproceedia.org
Eccomas Proceedia SMART (2023) 107-118

ECCOMAS
Proceedia

X ECCOMAS Thematic Conference on Smart Structures and Materials
SMART 2023
D.A. Saravanos, A. Benjeddou, N. Chrysochoidis and T. Theodosiou (Eds)

REVISITING MULTIDISCIPLINARY TIME-OF-ARRIVAL ESTIMATION METHODS FOR IMPACT DETECTION ON PLATES

LUKAS GRASBOECK*, ALEXANDER HUMER† AND AYECH BENJEDDOU‡

*Linz Center of Mechatronics GmbH, Linz, Austria
e-mail: lukas.grasboeck@lcm.at

† Institute of Technical Mechanics
Johannes Kepler University, Linz, Austria
e-mail: alexander.humer@jku.at

‡ Institut Supérieur de Mécanique de Paris, Saint Ouen, France
Université de Technologie de Compiègne, Roberval, Compiègne, France
e-mail: ayech.benjeddou@isae-supmeca.fr

Abstract. In the framework of guided waves propagation (GWP), different methods for estimating the time-of-arrival (TOA) of waves excited by impacts on carbon fiber-reinforced polymer (CFRP) plates are assessed. The TOA estimation is an essential ingredient of impact localization and quantification. To detect and measure the propagation of waves, piezoceramic patch sensors are surface-bonded to the plate. The plate is impacted at different locations using an impact hammer and an impact gun. The latter provides information about the energy introduced into the impacted structure. The GWP in thin-walled structures is a very complex and challenging phenomenon in many respects, in particular for anisotropic and multilayer materials. Therefore, this contribution revisits selected TOA estimation methods from two different fields of application: Akaike Information Criterion (AIC) (information theory) and Continuous Wavelet Transform (CWT) (signal processing). The aim is to give practical guidelines of how they can be applied to sensor data from plates under impact-induced GWP, and to identify their individual advantages and disadvantages in order to arrive at reliable TOA estimates, hence the plate's impact detection. The proposed investigations are based on experiments on an anisotropic (laminated CFRP) plate. The results indicate that the AIC method is capable of producing accurate and robust estimates of the onset time, even when faced with varying conditions such as changes in impact location, different types of impact, and variations in a method-specific parameter. The estimated values can be verified using CWT to determine the frequency components of the wave propagation that they correspond to, which may be very useful for a subsequent impact localization task.

Key words: time-of-arrival estimation, impact detection, Lamb waves, anisotropic plate, Akaike Information Criterion, Continuous Wavelet Transform

Peer-review under responsibility of the organizing committee of SMART 2023.
doi: 10.7712/150123.9769.451409

1 INTRODUCTION

The detection, localization, and assessment of impacts on load-bearing structures are crucial tasks in the field of structural health monitoring (SHM). The detection and localization of impacts are typically considered as passive processes, as no external actuation is required. The impact itself induces elastic waves that propagate through a structure and are captured by sensors. In thin-walled structures, guided waves are the most common form of wave propagation (see, e.g., [1, 2]). However, regardless of the actual impact localization method used, accurately detecting an impact is fundamental. This involves determining the time at which waves induced by an impact are captured by a sensor - referred to as the TOA. It is important to note that we distinguish between the commonly used term time-of-flight (TOF) and TOA. The TOF refers to the time it takes for the wave to propagate from the point of impact to a specific sensor, while the TOA references the time instance when the wave reaches the sensor. The TOA refers to a specific point in time, whereas the TOF denotes a time interval.

The goal of this research is to investigate selected TOA-estimation methods, which are well-established in their respective applications, in the context of impact monitoring of thin-walled structures. To achieve this, we make use of the AIC method, a statistical model selection method from information theory, to select the most appropriate TOA estimation. Additionally, we utilize the CWT method, which provides information about the spectral content over time by convolving the sensor signal with a collection of scaled wavelet functions. This additional information allows to bypass the complexity introduced by the dispersive nature of the GWP.

In the following, Section 2 describes the experimental setup and how the impact-related sensor signals are obtained. Section 3 recalls the fundamentals of the selected TOA estimation methods and how to estimate the TOA, given a sensor signal. Finally, in Section 4, we apply the TOA estimation techniques to the sensor signals obtained by impact hammer and impact gun on a laminated CFRP plate, and present the corresponding results.

2 EXPERIMENTAL SETUP

The structure used to investigate impact induced GWP is a quasi-isotropic CFRP plate of dimensions $1000\,\mathrm{mm} \times 1000\,\mathrm{mm} \times 2\,\mathrm{mm}$. It consists of seven plies of different thicknesses composed into a laminate of the form $[(0/90)_\mathrm{f} \,/\, +45 \,/\, -45 \,/ (\overline{0/90})_\mathrm{f}]_\mathrm{S}$ (outer fabrics: $0.4\,\mathrm{mm}$, center fabric: $0.2\,\mathrm{mm}$ and unidirectional layers: $0.25\,\mathrm{mm}$). The dispersion characteristics of the plate are determined by an air-coupled ultrasonic technique in the work of Schmidt et al. [3] for several directions. For the $0°$-direction, the dispersion curves are given for the fundamental Lamb wave modes, i.e., A_0 and S_0, in Figure 1 for both phase- and group wave velocities. The focus lies on impacts, which a structure experiences during its operation. Therefore, they are conducted with a hand-held instrumented impact hammer (PCB 086C03 from *PCB Piezotronics*) and an impact gun. The latter is specifically designed for material testing by generating an impact with a defined energy level using compressed air [4].

As our goal is not to damage the plate, we set the adjustable impact energy of the impact gun as small as possible, i.e., for this particular gun $7\,\mathrm{J}$. The GWP caused by the impacts are

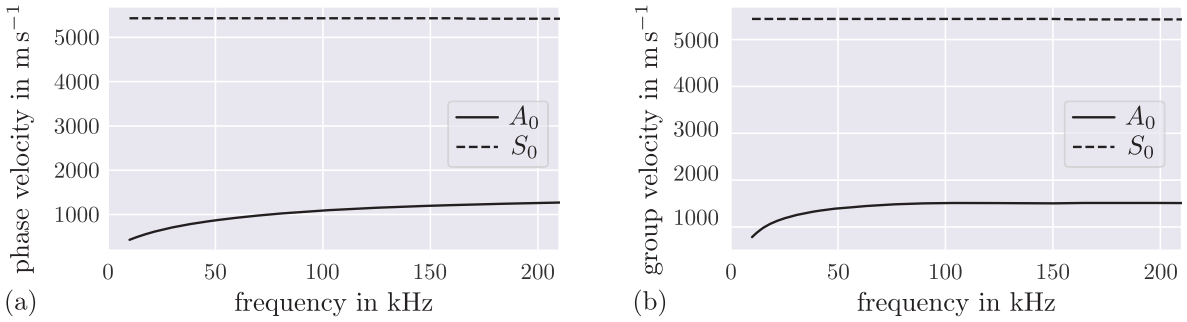

Figure 1: Dispersion characteristics of the CFRP plate in the frequency domain of interest in terms of phase velocity (a) and group velocity (b) for the 0°-direction.

measured with piezoceramic patch sensors (P-876.SP1 from *PI Ceramic*), which are surface-bonded to the plate. An overview of impact and sensor positions, as well as a picture of the used impact gun is provided in Figure 2. Additionally, the distances between sensor patches and

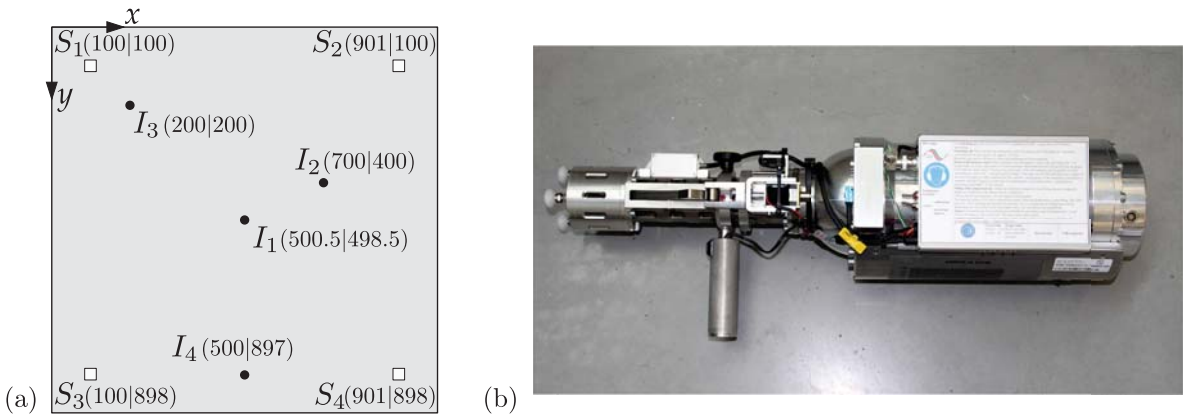

Figure 2: Positions of sensors (S_i; i = 1-4), i.e., their respective centers of the patches, and impacts (I_j; j = 1-4) on free CFRP plate (a) (all specified coordinates are in mm). A picture of the impact gun used for our experimental investigations (b).

impact hits are listed in Table 1. For the impact tests, the CFRP plate is placed on a foam mat. The output of the sensors are acquired using the NI PXIe-1085 data acquisition system from *National Instruments Corp.* with 12-bit resolution and a sampling rate of 1 MHz, resulting in a constant time increment of $\Delta t = 1\,\mu s$. In the measurements with the impact gun, a probe was used to amplify the amplitude with a factor of 1:25 in order to protect the data acquisition system from the high voltage outputs of the sensors. In our case, low-velocity impacts typically excite a broad but low frequency range (within the context of SHM). As a result, it is sufficient for our application to consider frequencies up to 100 kHz. This frequency range has been verified by a detailed analysis using FFT and CWT.

Table 1: Distances (in mm) between sensor patches and impact locations of the CFRP plate.

	S_1	S_2	S_3	S_4
I_1	564.9	564.9	565.7	565.7
I_2	670.8	361.1	779.7	537.0
I_3	141.4	708.1	705.1	989.2
I_4	891.7	892.2	400.0	401.0

3 METHODS UNDER INVESTIGATION

To estimate the TOA for guided waves in plates, we first need to understand what TOA means in this specific problem. Unlike in SHM applications, where excitation is well-defined and narrow-banded, the impact on the structure in our problem is relatively broadband [2]. Additionally, for thin-walled structures where Lamb waves propagate, the response spectrum differs significantly from the spectrum of the impact load. Because Lamb waves with different frequencies propagate at different speeds due to the dispersive nature of waves in 3D continua, there is no single TOA. Instead, we need to be specific about particular frequencies, since waves of different frequencies arrive at different times. Our goal is to use the TOA estimation as a means for impact detection, localization, and quantification. While the dispersive nature of Lamb waves may seem like an additional complication, we can use that knowledge to our advantage, if we know the dispersion properties of the structure.

3.1 Akaike information criterion

The AIC algorithm for TOA estimation was successfully applied on sensor signals of seismic events to detect the onset-time of seismic waves. It is based on the assumption that the non-stationary sensor signal can be modeled as a sequence of locally stationary processes, modeled as autoregressive processes [5]. On the subject of TOA estimation, we distinguish between two locally stationary segments, i.e., the non-informative part (noise) and the informative part (signal) [5, 6]. The time sample, which separates these two segments, is indicated by the minimum value of the AIC and is therefore the TOA we are looking for. To avoid the determination of the autoregressive coefficients, Maeda [7] has developed a method to compute the AIC directly from the signals. The AIC of a sensor signal $s(t_i)$ of N samples is given as

$$\chi(t_i) = i \ln\left(\mathrm{var}\left\{s(t_j)|_{j=0\ldots i}\right\}\right) + (N-i-1)\ln\left(\mathrm{var}\left\{s(t_j)|_{j=i+1\ldots n}\right\}\right) \ , \tag{1}$$

where i is the running index through all time steps of the signal $s(t_i)$ and $\mathrm{var}\{\cdot\}$ denotes the variance. It is essential that only a segment of the sensor signal is used for the calculation of AIC (1), to correctly estimate the TOA. Which part of the signal is used for this purpose will be determined by the so-called *AIC pickers*. We adopt the AIC picker used by Sedlak et al. [5], who in turn used a modified version of the seismogram threshold picker of Allen [8]. The used AIC picker is modified for thin plates

$$\beta(t_i) = |s(t_i)| + R_a|s(t_i) - s(t_{i-1})|, \tag{2}$$

where R_a should be close to 1 for artificial AE events (e.g. pencil-lead break test) and close to 4 for real AE sources with low signal-to-noise-ratio (SNR) [5]. The AIC algorithm consists of two steps: (i) define a time-window with the AIC picker and (ii) calculate AIC (Eq. (1)) of the specified section of the signal. Once this is done, we get a first estimate of the TOA by picking the time-instance of the global minimum of $\chi(t_i)$ [5], i.e.,

$$\hat{t} = \arg\min\left(\chi\left(t_i\right)\right). \tag{3}$$

We repeat these two steps in an even smaller window (second AIC window) around the first estimate, i.e., we apply a second estimate of the TOA to increase the accuracy of the AIC algorithm [9]. The minimum of the repeated application of Eq. (1) gives the desired TOA.

The first step of the AIC algorithm involves defining a window, called the first AIC window, between the lower and upper bound values of $0\,\mathrm{s}$ and $t_{\max} + t_{\mathrm{am}}$, where $t_{\max}$ is the time-instance of the maximum of $\beta(t_i)$ and t_{am} is a time delay added to $t_{\max}$. The value of t_{am} recommended for thin plate specimens is usually set to $20\,\mu\mathrm{s}$. Using Eq. (1) on the time interval defined by the first AIC window gives the first estimate of TOA, denoted by t_{fe}. The second step of the algorithm focuses on the immediate vicinity of the first estimate t_{fe}. For this purpose, the second AIC window is defined as two parts of length t_{fb} and t_{fa}, which describe the lengths of the window parts before and after t_{fe}, with lower and upper bounds of $t_{\mathrm{lb2}} = t_{\mathrm{fe}} - t_{\mathrm{fb}}$ and $t_{\mathrm{ub2}} = t_{\mathrm{fe}} + t_{\mathrm{fa}}$, respectively. In recent literature, the width of the second AIC window, which is $t_{\mathrm{fb}} + t_{\mathrm{fa}}$, was determined through a trial-and-error process. According to recommendations from the same literature, it is advisable to select t_{fb} and t_{fa} values of $10\,\mu\mathrm{s}$ and $30\,\mu\mathrm{s}$, respectively [6]. However, for our application, different parameter values of the AIC algorithm have to be chosen to determine the TOA with sufficient accuracy. Figure 3 illustrates the two-step procedure of the AIC algorithm based on the output of sensor S_2 for I_3.

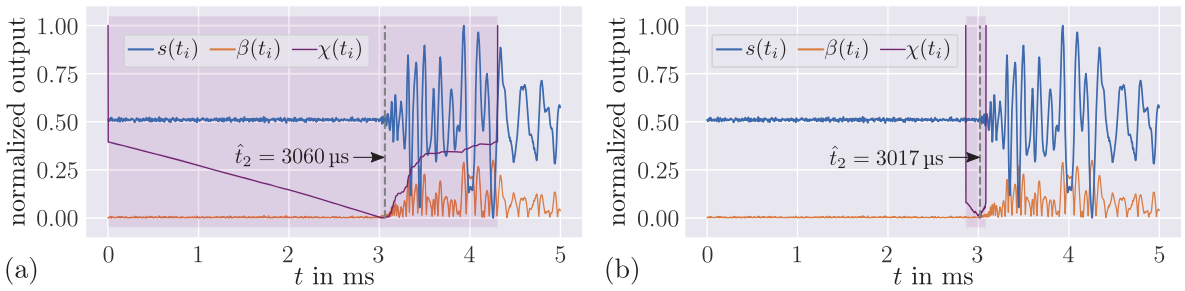

Figure 3: Illustration of AIC's two-step-procedure to determine the TOA based on the signal of S_2 of hammer impact I_3. The purple area indicates the window, where the AIC, i.e., $\chi(t_i)$, is applied on the signal. In the first AIC step (a), the AIC window is determined by the AIC picker via the characteristic function $\beta(t_i)$ (Eq. (2)) and in the second AIC step (b) the TOA estimation is repeated in a small time domain around the first estimate.

3.2 Continuous wavelet transform

Wave speed in dispersive media being frequency-dependent, we can use time-frequency analysis (TFA) methods for the TOA estimation. TFA methods allow to analyze the spectral content of a sensor signal's frequency and infer information on the distance traveled. One prominent representative of TFA is the CWT. However, as for every TFA method, a compromise between resolution in time and frequency domain must be made. The CWT has the advantage of multi-resolution, allowing for varying resolution in time and frequency. To perform a CWT of a signal $s(t)$, a "dictionary" of wavelets is generated based on the scaling and shifting parameters a and b of the mother wavelet $\psi(t)$. The CWT of a signal $s(t)$ and the scaled and shifted mother wavelet are defined as

$$\mathcal{W}_\psi\{s\}(a,b) = \int_{-\infty}^{\infty} \psi_{a,b}^* s(t) dt, \qquad \psi_{a,b}(t) = \frac{1}{\sqrt{a}} \psi \left(\frac{t-b}{a} \right), \tag{4}$$

where $\psi_{a,b}$ denotes the shifted and dilated mother wavelet [10]. The resulting set of wavelet coefficients, $\mathcal{W}_\psi\{s\}(a,b)$, represents a highly redundant time-frequency image of the signal [10, p. 17]. The square modulus of the wavelet coefficients, i.e., the scalogram, provides information about the energy density in the time-frequency domain and can be used to estimate the TOA and wave speed of the wave propagation

$$|\mathcal{W}_\psi\{s\}(a,b)|^2 = |\mathcal{W}_\psi\{s\}(a,b)| \, |\mathcal{W}_\psi\{s\}(a,b)^*|. \tag{5}$$

The frequency information obtained from the scalogram allows the estimation of the wave speed based on the dispersion characteristics of the material being tested, which is useful in locating the impact that caused the wave propagation. While the literature has used the global maximum of the scalogram to determine the TOA, we found that using local maxima of scalogram sections without prior knowledge of the sensor signal also provides reasonable results.

4 TIME-OF-ARRIVAL ESTIMATION RESULTS

In what follows, the sensor signals generated by waves after impacts on the CFRP plate will be analyzed using the TOA estimation methods discussed in Section 3. The precise determination of the TOA as a starting point for impact localization is one aspect. However, it must also be ensured that, with regard to dispersive wave propagation, waves of the same frequency are detected. If this is not the case, different propagation speeds are assumed, which falsifies the result of the localization. Fiber-reinforced plastics, in particular, present an additional complication in this context, with regard to the material-induced continuous mode conversion [3].

In the AIC method, there are several parameters that can be adjusted. The size of the AIC windows, particularly the second one (defined by t_{fb} and t_{fa}), has a significant impact on the method's sensitivity. To obtain the most robust results, the parameter t_{fb} should be chosen in the second AIC step so that a sufficiently large segment of the signal remains, that is not related to the wave propagation caused by the impact. To demonstrate this, we provide results of TOA

estimations for different values of t_{fb} (varying from $4\,\mu\mathrm{s}$ to $500\,\mu\mathrm{s}$) for all sensor signals and impact positions, depicted in Figure 4. To evaluate the accuracy of the results, we compare them to manually determined TOA values $\bar{t}$, which are considered as to be correct. In general, the results show a small discrepancy to the manually determined TOA when t_{fb} is set above $150\,\mu\mathrm{s}$. However, for sensor S_3 at impact I_3, early estimates are observed when t_{fb} exceeds $365\,\mu\mathrm{s}$.

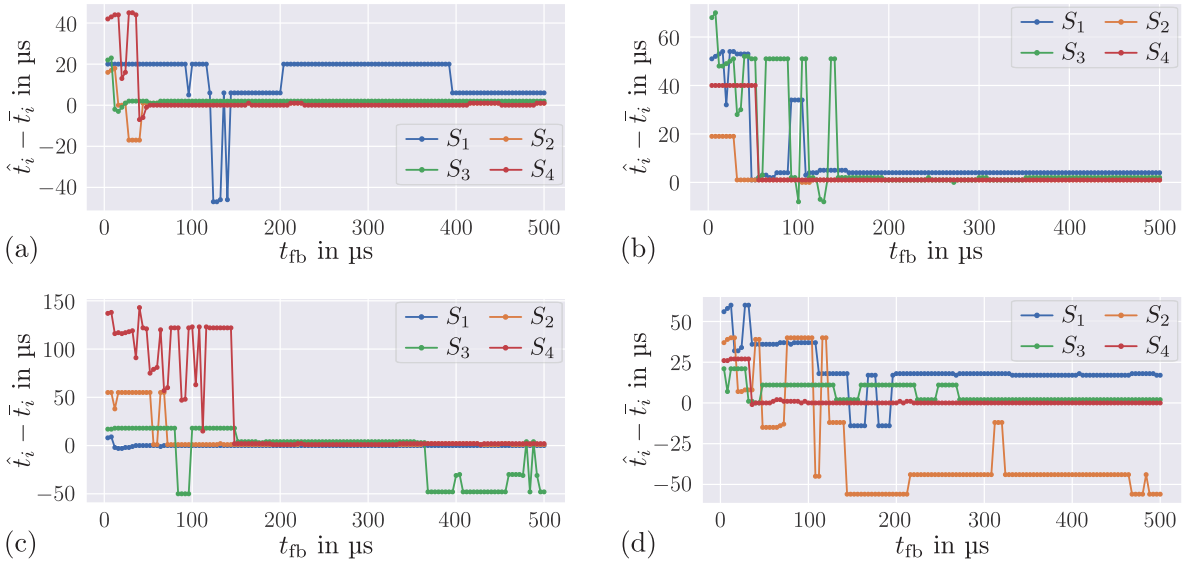

Figure 4: Sensitivity of TOA estimation results for different values of lower bound of second AIC window t_{fb}. The results are visualized as differences to the "true" (manually determined) TOA, i.e., $\bar{t}$. Subfigures (a) to (d) correspond to impacts I_1 to I_4.

Moreover, for sensor S_2 at impact I_4, a suitable value for t_{fb}, that accurately estimates the TOA of the wave, cannot be determined with confidence. Determining the TOA can be challenging, particularly for sensor signals with a slow transition from noise to the signal, i.e., where the rise in amplitude is very subtle. This difficulty is observed in both the AIC method and manual TOA determination. Upon closer examination of the signal from sensor S_2 at impact I_4 for three distinct t_{fb} values ($200\,\mu\mathrm{s}$, $300\,\mu\mathrm{s}$ and $315\,\mu\mathrm{s}$), the AIC method demonstrates a high sensitivity to the selected t_{fb} values, see Figure 5. Here, we can clearly see how small the differences between the local minima and the global minimum of $\chi(t_i)$ are. These differences between the minima change for different values of t_{fb}, leading to different estimates of the TOA. Since we know the time of impact during the experiments with the hammer impact t_{imp} (which would not be the case in a real-world application), we can calculate the time difference between the time of impact and all estimated TOA values, i.e., all estimations with $t_{\mathrm{fb}} \geq 150\,\mu\mathrm{s}$. Together with the distance of the sensors ($\mathrm{S}_i;\ i = 1\text{-}4$) from the impacts ($I_j;\ j = 1\text{-}4$), we can estimate a wave propagation velocity $\hat{v}_i^j$. In addition, we can compare this with the manually determined TOA

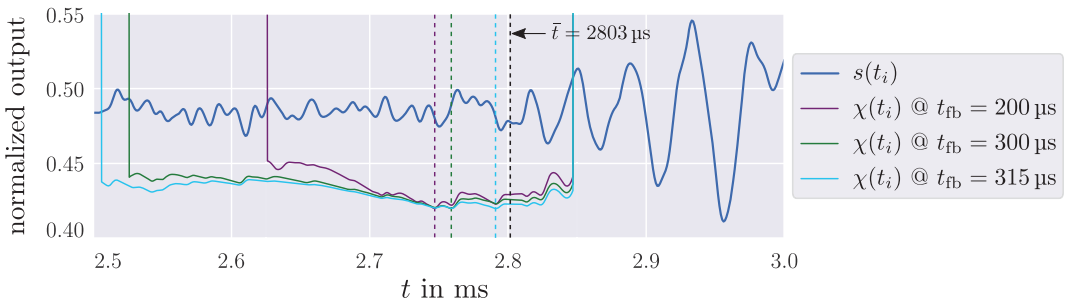

Figure 5: Plot of $\chi(t_i)$ for different values of t_{fb} for the signal of sensor S_2 upon impact I_4. The dashed lines mark the estimated TOA in the second AIC step: $\hat{t} = 2747\,\mu s$, $\hat{t} = 2759\,\mu s$ and $\hat{t} = 2791\,\mu s$ for $t_{\mathrm{fb}} = 200\,\mu s$, $t_{\mathrm{fb}} = 300\,\mu s$ and $t_{\mathrm{fb}} = 315\,\mu s$, respectively. The manually determined "true" TOA is estimated to $\bar{t} = 2803\,\mu s$.

values and calculate a respective "true" wave propagation velocity $\bar{v}_i^j$

$$\hat{v}_i^j = \frac{d_i^j}{\hat{t} - t_{\mathrm{imp}}}, \qquad \bar{v}_i^j = \frac{d_i^j}{\bar{t} - t_{\mathrm{imp}}}. \tag{6}$$

The values of this comparison are listed in Table 2. As the TOA was calculated for many different values of t_{fb}, a range of estimated TOA values is obtained accordingly (indicated by $[\cdot]$). If only one value is given, a constant TOA value is estimated for the entire parameter range of t_{fb}. The sensor signals together with the impact force signal are given in Figures 6 and 7 for impact positions I_2 and I_3, respectively.

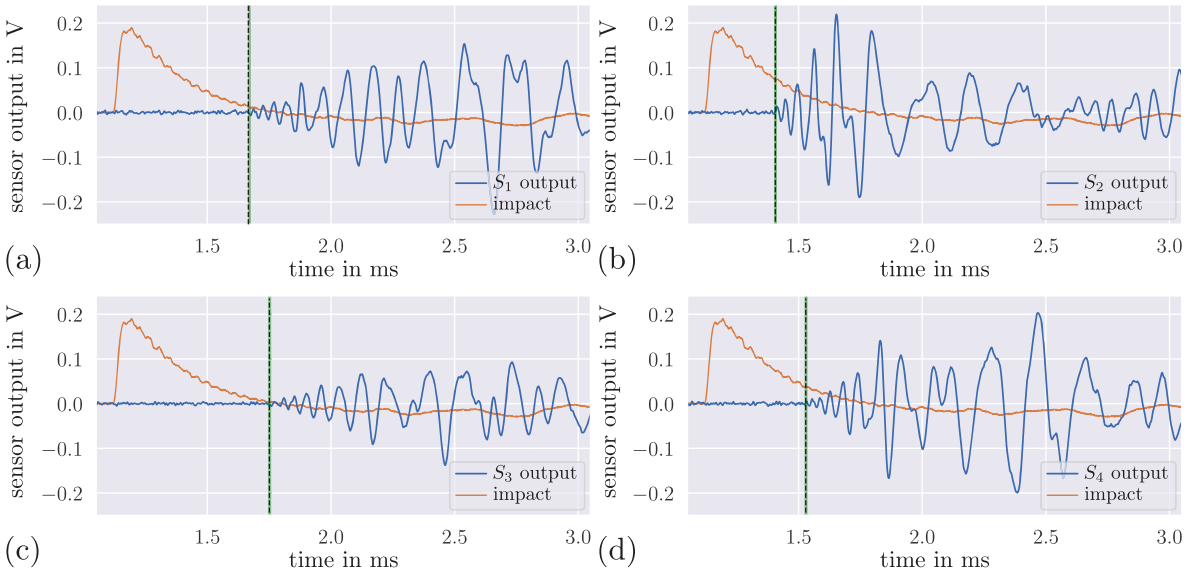

Figure 6: Output of sensors together with hammer impact and manually determined TOA (=dashed black line) for impact I_2. The area shaded in green corresponds to the range of TOA estimates obtained for values of $t_{\mathrm{fb}} \geq 150\,\mu s$.

Table 2: The range of estimated TOA values (for the parameter range of $t_{\mathrm{fb}} \geq 150\,\mu\mathrm{s}$), denoted as $\hat{t}$, along with their estimated wave speeds $\hat{v}_i^j$ for impacts with the impact hammer. The results are obtained by the AIC method with parameters $R_a = 1$, $t_{\max} = 50\,\mu\mathrm{s}$, $t_{\mathrm{lb1}} = 0\,\mu\mathrm{s}$ and $t_{\mathrm{fa}} = 25\,\mu\mathrm{s}$. The estimation results are compared to the manually determined "true" TOA values, denoted as $\bar{t}$, and their associated wave speeds $\bar{v}_i^j$.

Impact	Sensor	$\hat{t}$ in µs	$\hat{v}_i^j$ in $\mathrm{m\,s^{-1}}$	$\bar{t}$ in µs	$\bar{v}_i^j$ in $\mathrm{m\,s^{-1}}$
I_1	S_1	[2561, 2575]	[1092.8, 1123.2]	2555	1136.8
	S_2	2563	1118.8	2562	1121.0
	S_3	2568	1109.2	2566	1113.6
	S_4	[2572, 2573]	[1098.4, 1100.6]	2572	1100.6
I_2	S_1	[1670, 1671]	[1219.7, 1221.9]	1666	1230.9
	S_2	1407	1262.6	1406	1267.1
	S_3	[1751, 1753]	[1233.8, 1237.7]	1751	1237.7
	S_4	1530	1313.0	1529	1316.3
I_3	S_1	2616	1386.5	2616	1386.8
	S_2	[3017, 3018]	[1405.0, 1407.8]	3016	1410.6
	S_3	[3007, 3059]	[1293.8, 1430.3]	3055	1303.4
	S_4	[3310, 3311]	[1241.2, 1242.8]	3309	1244.3
I_4	S_1	[2831, 2863]	[1156.6, 1206.7]	2845	1184.3
	S_2	[2747, 2791]	[1276.4, 1362.1]	2803	1254.8
	S_3	[2373, 2382]	[1379.3, 1423.5]	2371	1433.7
	S_4	[2379, 2380]	[1392.4, 1397.2]	2379	1397.2

The range of TOA estimations obtained for values of $t_{\mathrm{fb}} \geq 150\,\mu\mathrm{s}$ is indicated by the green shaded area. Based on the results obtained from the hammer impact experiments, we can conclude that the TOA estimations work very robustly and correspond to the manually determined values. However, it is noticeable that the farther the sensor is from the impact, the more is the spread of TOA estimation. Furthermore, it should be noted that even with the manually determined TOA values, there is variation of the resulting wave speeds among impacts. Similarly, these values vary among individual sensors for a particular impact. By using the CWT, we can analyze the frequency content of the sensor signals over time. This is exemplified by the scalogram of sensor S_2 of hammer impact I_2 in Figure 8, by using the Morlet wavelet centered at $\omega_c = 5\,\mathrm{rad\,s^{-1}}$. When examining the scalogram at various frequencies, the first arrival of an "impact-related" sensor signal is manifested as a (first) local maximum. Comparing the estimated TOA values obtained by AIC with the positions of the local maxima of the scalogram sections, gives insight which frequency content of the wave propagation is detected by AIC. This can be used to verify whether the AIC method estimates TOA values which correspond to the same frequency of the wave propagation. If the latter is ensured, the same wave propagation velocity can be assumed for, e.g., a subsequent impact localization task.

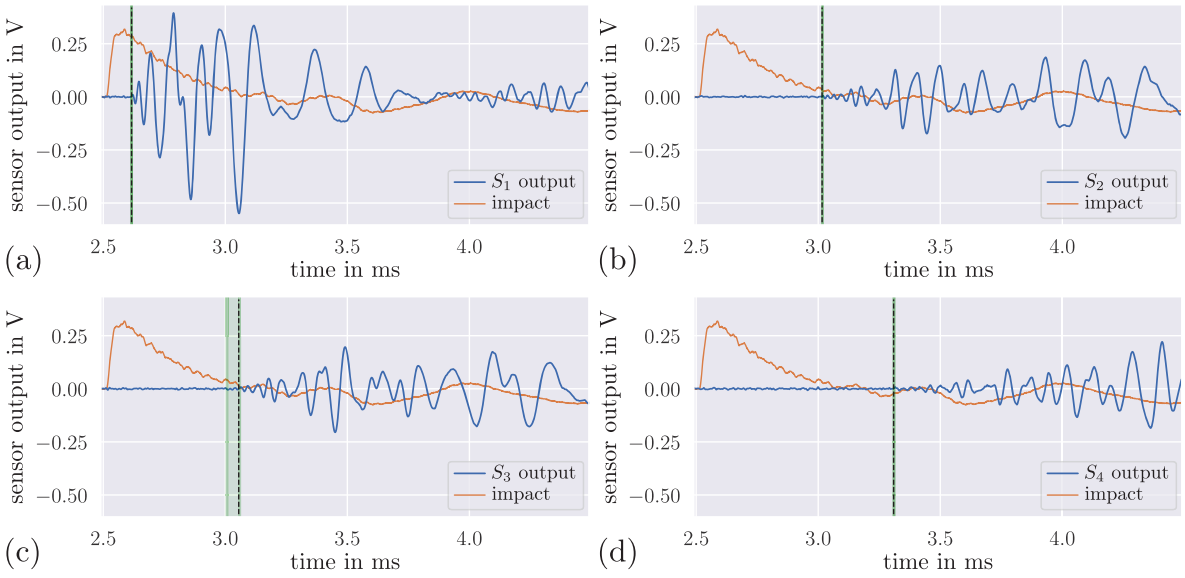

Figure 7: Output of sensors together with hammer impact and manually determined TOA (=dashed black line) for impact I_3. The area shaded in green corresponds to the range of TOA estimates obtained for values of $t_{\mathrm{fb}} \geq 150\,\mu\mathrm{s}$.

If not, the wave propagation velocities can be corrected using the dispersion properties of the group velocity of the material under test, if necessary. Based on the estimated wave speed of the hammer impact and the dispersion characteristics of the CFRP plate (Figure 1), it is concluded that the TOA can only be estimated based on the fundamental A_0 mode.

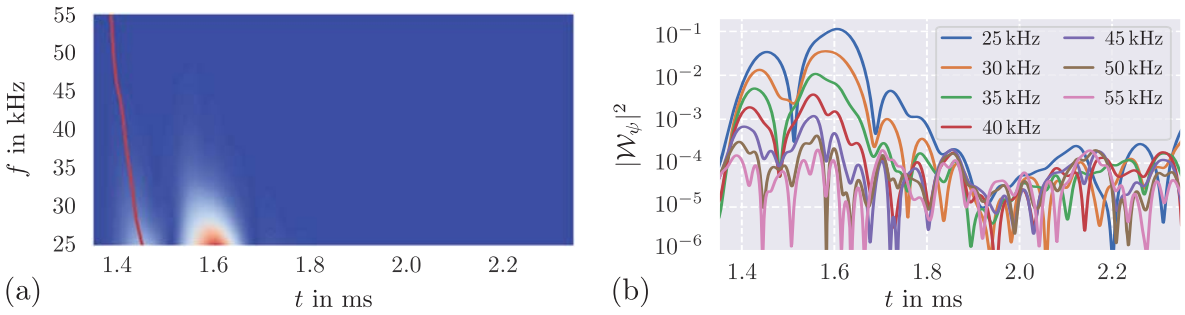

Figure 8: Scalogram of sensor signal S_2 for impact I_2. The normalized square of the CWT's absolute value is illustrated in a time interval of 1 ms and a frequency range of 25 kHz to 55 kHz. The red line shows the location of first (local) maximum values of the scalogram in the time-domain as a function of the frequency (a). Sections of scalogram at 25 kHz, 30 kHz, 35 kHz, 40 kHz, 45 kHz, 50 kHz and 55 kHz: The first local maximum at 45 kHz is located at 1403 µs, which indicates that the AIC method ($\hat{t} = 1407\,\mu\mathrm{s}$) detects the TOA of a wave with 45 kHz (b).

Again, we use AIC with different t_{fb} values ranging from $4\,\mu\mathrm{s}$ to $500\,\mu\mathrm{s}$ to analyze the sensor data from impact tests conducted with the impact gun. In these measurements, since the point in time of the impacts are unknown, one is approaching the conditions of reality to some extent. The resulting range of TOA estimates and the manually determined values are presented in

Table 3. As with the results from the impact hammer, we also see a wider spread in the estimated values for sensors that are further away from the impact, e.g. S_3 & S_4 @ Impact I_3 and S_1 & S_2 @ Impact I_4.

Table 3: The range of the estimated TOA values, denoted as $\hat{t}$, is given for the parameter range of $t_{\mathrm{fb}} \geq 170\,\mu\mathrm{s}$, for impacts with the impact gun. The results are obtained by the AIC method with parameters $R_a = 1$, $t_{\max} = 50\,\mu\mathrm{s}$, $t_{\mathrm{lb1}} = 0\,\mu\mathrm{s}$ and $t_{\mathrm{fa}} = 25\,\mu\mathrm{s}$. The estimation results are compared to the manually determined "true" TOA values, denoted as $\bar{t}$.

Impact	Sensor	$\hat{t}$ in µs	$\bar{t}$ in µs
I_1	S_1	[2363, 2382]	2360
	S_2	2368	2348
	S_3	[2382, 2383]	2369
	S_4	2367	2371
I_2	S_1	2307	2284
	S_2	2083	2060
	S_3	[2478, 2479]	2476
	S_4	[2201, 2202]	2191

Impact	Sensor	$\hat{t}$ in µs	$\bar{t}$ in µs
I_3	S_1	[1620, 1637]	1620
	S_2	[2034, 2035]	2030
	S_3	[1996, 2049]	2010
	S_4	[2323, 2324]	2308
I_4	S_1	[2814, 2815]	2804
	S_2	[2840, 2841]	2831
	S_3	[2415, 2416]	2412
	S_4	[2412, 2426]	2409

5 CONCLUSIONS

The main objective of this study is to accurately estimate the TOA of impacts on a CFRP plate using an impact hammer and an impact gun. The AIC method has demonstrated high robustness in this specific application, providing reliable results despite variations in impact location and device. Specifically, the choice of the AIC window in the second AIC step does not significantly affect the accuracy of TOA estimation. The estimated values can be verified using CWT to determine the frequency components of the wave propagation that they correspond to, ensuring that TOA values with the same frequency components are compared. If the TOA values correspond to different frequencies, the results can be corrected using dispersion properties. However, it is challenging to estimate the TOA for sensor signals that have a slow transition from noise to the "impact-related" signal, especially for sensors located far from the impact location. Future investigations will focus on improving the accuracy and reliability of the TOA estimation for these sensor signals. We then turn to impact localization methods using the proven TOA estimation methods.

6 ACKNOWLEDGMENTS

This work has been supported by the COMET-K2 Center of the Linz Center of Mechatronics (LCM) funded by the Austrian federal government and the federal state of Upper Austria. The authors would like to thank the Institute of Lightweight Systems of the German Aerospace Cen-

ter (DLR) for the support during the research stay, particularly for the opportunity to conduct a part of the work at DLR.

REFERENCES

[1] H. Lamb, "On waves in an elastic plate," *Proceedings of the Royal Society of London. Series A, Containing Papers of a Mathematical and Physical Character*, vol. 93, no. 648, pp. 114–128, 1917.

[2] V. Giurgiutiu, *Structural health monitoring with piezoelectric wafer active sensors*, 2nd ed. Amsterdam: Academic Press/Elsevier, 2014.

[3] D. Schmidt, C. Heinze, W. Hillger, A. Szewieczek, M. Sinapius, and P. Wierach, "Design of mode selective actuators for Lamb wave excitation in composite plates," in *Health Monitoring of Structural and Biological Systems 2011*, T. Kundu, Ed., vol. 7984, International Society for Optics and Photonics. SPIE, 2011.

[4] "Ingenieurtechnische Dienstleistungen," https://web.archive.org/web/20220529011729/https://www.id-lindner.de/en/sonderentwicklungen#, accessed: 2023-03-31.

[5] P. Sedlak, Y. Hirose, and M. Enoki, "Acoustic emission localization in thin multi-layer plates using first-arrival determination," *Mechanical Systems and Signal Processing*, vol. 36, no. 2, pp. 636–649, 2013.

[6] J. Akram and D. W. Eaton, "A review and appraisal of arrival-time picking methods for downhole microseismic data," *Geophysics*, vol. 81, no. 2, pp. KS71–KS91, 2016.

[7] N. Maeda, "A method for reading and checking phase time in auto-processing system of seismic wave data," *Zisin (Journal of the Seismological Society of Japan. 2nd ser.)*, vol. 38, no. 3, pp. 365–379, 1985.

[8] R. Allen, "Automatic phase pickers: Their present use and future prospects," *Bulletin of the Seismological Society of America*, vol. 72, no. 6B, pp. S225–S242, 1982.

[9] M. E. de Simone, F. Ciampa, S. Boccardi, and M. Meo, "Impact source localisation in aerospace composite structures," *Smart Materials and Structures*, vol. 26, no. 12, 2017.

[10] S. G. Mallat, *A wavelet tour of signal processing: The Sparse way*, 3rd ed. Amsterdam: Elsevier /Academic Press, 2009.